Estimation of the Antarctic surface mass balance using MAR (1979-2015) and identification of dominant processes

Cécile Agosta[1,2,3], Charles Amory[1], Christoph Kittel[1], Anais Orsi[2], Vincent Favier[3], Hubert Gallée[3], Michiel R. van den Broeke[4], Jan T. M. Lenaerts[4,5], Jan Melchior van Wessem[4], and Xavier Fettweis[1]

[1]F.R.S.-FNRS, Laboratory of Climatology, Department of Geography, University of Liège, B-4000 Liège, Belgium
[2]Laboratoire des Sciences du Climat et de l'Environnement (IPSL/CEA-CNRS-UVSQ UMR 8212), CEA Saclay, F-91190 Gif-sur-Yvette, France
[3]Université Grenoble Alpes, CNRS, Institut des Géosciences de l'Environnement, F-38000, Grenoble,France
[4]Institute for Marine and Atmospheric Research Utrecht, Utrecht University, Utrecht, the Netherlands
[5]Department of Atmospheric and Oceanic Sciences, University of Colorado Boulder, Boulder CO, United States of America

Correspondence: Cécile Agosta (cecile.agosta@gmail.com)

Abstract. The Antarctic ice sheet mass balance is a major component of the sea level budget and results from the difference of two fluxes of a similar magnitude: ice flow discharging in the ocean and net snow accumulation on the ice sheet surface, i.e. the surface mass balance (SMB). Separately modelling ice dynamics and surface mass balance is the only way to project future trends. In addition, mass balance studies frequently use regional climate models (RCMs) outputs as an alternative to observed fields because SMB observations are particularly scarce on the ice sheet. Here we evaluate new simulations of the polar RCM MAR forced by three reanalyses, ERA-Interim, JRA-55 and MERRA2, for the period 1979-2015, and we compare our results to the last outputs of the RCM RACMO2 forced by ERA-Interim. We show that MAR and RACMO2 perform similarly well in simulating coast to plateau SMB gradients, and we find no significant differences in their simulated SMB when integrated over the ice sheet or its major basins. More importantly, we outline and quantify missing processes in both RCMs. Along stake transects, we show that both models accumulate too much snow on crests, and not enough snow in valleys, as a result of erosion-deposition processes not included in MAR, where the drifting snow module has been switched off, and probably underestimated in RACMO2 by a factor of three. As a consequence, the amount of drifting snow sublimating in the atmospheric boundary layer remains a potentially large mass sink needed to be better constrained. Moreover, MAR generally simulates larger SMB and snowfall amounts than RACMO2 inland, whereas snowfall rates are significantly lower in MAR than in RACMO2 at the ice sheet margins. This divergent behaviour at the margins results from differences in model parameterisations, as MAR explicitly advects precipitating particles through the atmospheric layers and sublimates snowflakes in the undersaturated katabatic layer, whereas in RACMO2 precipitation is added to the surface without advection through the atmosphere. Consequently, we corroborate a recent study concluding that sublimation of precipitation in the low-level atmospheric layers is a significant mass sink for the Antarctic SMB, as it may represent ~240±25 Gt yr^{-1} of difference in snowfall between RACMO2 and MAR for the period 1979-2015, which is 10% of the simulated snowfall loaded on the ice sheet and more than twice the surface snow sublimation as currently simulated by MAR.

1 Introduction

Mass loss from the Antarctic ice sheet (AIS) and therewith its contribution to the sea level budget results from the difference of two fluxes of a similar magnitude: ice flow discharging in the ocean (D) and net snow accumulation on the ice sheet surface, i.e. the surface mass balance (SMB). The total ice sheet mass balance (SMB minus D) can be assessed using several approaches
5 (Shepherd et al., 2012), but separately modelling ice dynamics and surface mass balance, called the input-output method, is the only way to project future trends.

Surface mass balance as used in this study is the sum of mass gains (mainly snowfall accumulation and some riming), mass losses (mainly surface and drifting snow sublimation, some liquid water runoff) and redistribution of snow by the wind, which can lead to either deposition (mass gain) or erosion (mass loss). Snowfall rates are one order of magnitude larger than all
10 of the other SMB fluxes at the continental scale (Lenaerts et al., 2012b), with the largest amounts found along the ice sheet margins due to cyclonic activity in the Southern Ocean and to the orographic lifting of relatively warm and moist air masses (van Wessem et al., 2014; Favier et al., 2017). Accumulation patterns are highly variable at the kilometre scale and from year to year (e.g., Agosta et al., 2012). Consequently, proper observations of SMB require a high spatial coverage (e.g. stake-lines, accumulation radars plus ice-cores for layer dating and snow density) and a temporal sampling spanning several years (Eisen
15 et al., 2008). Even if efforts have been made to fulfil those requirements, ground-based observations are scarce and carry with them high logistical costs in this cold, windy and remote environment. Interpolation techniques used to interpolate the scarce SMB observations (Vaughan et al., 1999; Arthern et al., 2006) encounter major caveats (Magand et al., 2008; Genthon et al., 2009; Picard et al., 2009).

This is why many AIS mass balance studies use output of regional climate models (RCMs) to estimate ice sheet SMB for
20 the recent decades (e.g., Rignot et al., 2011; Shepherd et al., 2012; Gardner et al., 2018). In order to obtain a good agreement with observations, atmospheric models require accurate large-scale circulation patterns together with a proper representation of snow surface processes, clouds, turbulent fluxes, and a relatively high horizontal resolution to properly resolve the complex ice sheet topography at the margins.

Here, we compare SMB fields of the state-of-the-art regional climate model RACMO2 (van Wessem et al., 2017) with new
25 simulations of the regional climate model MAR, applied here for the first time over the whole AIS but already widely used for polar studies, e.g. in Greenland (Fettweis et al., 2013, 2017), Svalbard (Lang et al., 2015), Adélie Land (Antarctic coastal area, Gallée et al., 2013; Amory et al., 2015) and Dome C (Antarctic plateau, Gallée et al., 2015). We use available SMB observational datasets to show that both MAR and RACMO2 perform similarly well in simulating the SMB field. In addition, we identify significant processes that still need to be included and/or improved in both RCMs.

30 In Section 2, we describe MAR and its specific set-up for Antarctica, together with RACMO2, the forcing fields, observational datasets and methods designed for model evaluation. In Section 3, we show that both RCMs share common biases against observed SMB, resulting from erosion-deposition processes. Secondly, we analyse SMB differences between models and show that many of the discrepancies can be attributed to low-level sublimation of precipitation in katabatic channels. Fi-

nally, in Section 4, we summarise our main findings and discuss further efforts to be achieved for a better assessment of the AIS surface mass balance.

2 Data and methods

2.1 Regional modelling

2.1.1 Regional atmospheric models

For the first time, the polar-oriented regional atmospheric model MAR is applied for decades-long simulations over the whole Antarctic ice sheet. MAR atmospheric dynamics are based on the hydrostatic approximation of the primitive equations, fully described in Gallée and Schayes (1994). Prognostic equations are used to depict five water species: specific humidity, cloud droplets and ice crystals, raindrops and snow particles (Gallée, 1995). Sublimation of airborne snow particles is a direct contribution to the heat and moisture budget of the atmospheric layer in which these particles are simulated. The radiative transfer through the atmosphere is parametrised as in Morcrette (2002), with snow particles affecting the atmospheric optical depth (Gallée and Gorodetskaya, 2010). The atmospheric component is coupled to the surface scheme SISVAT (soil ice snow vegetation atmosphere transfer, De Ridder and Gallée, 1998) dealing with the energy and mass exchanges between surface, snow and atmosphere. The snow–ice part of SISVAT is based on the snow model CROCUS (Brun et al., 1992). It is a one-dimensional multilayered energy balance model which simulates meltwater refreezing, snow metamorphism and snow surface albedo depending on snow properties. We used MAR version 3.6.4, simply called MAR here-after. In this version the physical settings are the same as in MAR version 3.5.2 used for Greenland (Fettweis et al., 2017), except for the adaptations detailed below.

Grid: Projection is the standard Antarctic polar stereographic (EPSG:3031). The horizontal resolution is 35 km, an intermediate resolution that results from a computation time compromise in order to run the model with multiple reanalyses and global climate model forcings over the 20th and the 21st century. The vertical discretisation is composed of 23 hybrid levels from ∼2 m to ∼17000 m above the ground.

Boundaries: The topography is derived from the Bedmap2 surface elevation dataset (Fretwell et al., 2013). Because the Antarctic domain is about 4 times larger than the Greenland domain, the circulation has to be more strongly constrained. This is why we use a boundary relaxation of temperature and wind in the upper atmosphere starting from 400 hPa (∼6000 m above the ground) to 50 hPa (upper level), as in van de Berg and Medley (2016), whereas relaxation starts from 200 hPa in Fettweis et al. (2017).

Parameterisations:

a) The fresh snow density ρ_s is computed as a function of 10 m wind speed ws_{10} (m s^{-1}) and surface temperature T_s (K):

$$\rho_s = 149.2 + 6.84\, ws_{10} + 0.48\, T_s, \tag{1}$$

with minimum-maximum values of 200–400 $\mathrm{kg\,m^{-3}}$. This parameterisation was defined so that the simulated density of the first 50 cm of snow fits observations collected over the Antarctic ice sheet (see Fig. S1, with snow density database detailed in Table S1).

b) The aerodynamic roughness length z_0 is computed as a function of the air temperature, as proposed in Amory et al. (2017). The parameterisation was tuned so that z_0 fit the observed seasonal variation between high (> 1 mm) summer and lower (0.1 mm) winter values in coastal Adélie Land, for air temperatures above -20 °C. For lower temperatures, z_0 is kept constant and set to 0.2 mm, in agreement with observed z_0 values on the Antarctic Plateau (e.g., Vignon et al., 2016);

c) As in Fettweis et al. (2017), drifting snow is not activated. Amory et al. (2015) shown that the drifting snow routine was sensitive to parameter choices. Given that an updated version of this routine is under evaluation against satellite and ground-based observations over the whole Antarctic ice sheet, we decided to switch off the drifting snow for our first Antarctic-scale MAR simulations.

We compare the MAR results over the AIS to the latest outputs of the regional atmospheric model RACMO2 version 2.3p2 (van Wessem et al., 2017), called RACMO2 here-after, using a horizontal resolution of 27 km and a vertical resolution of 40 atmospheric levels. This regional model is developed by the Royal Netherlands Meteorological Institute (KNMI), and has subsequently been adapted for modelling the Antarctic climate and its surface mass balance (van de Berg et al., 2006). It includes a snowdrift scheme (Lenaerts et al., 2012a), an albedo routine with prognostic snow grain size (Kuipers Munneke et al., 2011), and a multilayer snow model computing melt, percolation, refreezing and runoff (Ettema et al., 2010).

MAR and RACMO2 models were developed independently. We will not detail here the many physical parameterisation differences between both RCMs, but we will later highlight some of them we show having a significant impact on the modelled SMB.

2.1.2 Forcing reanalyses

Regional atmospheric models are forced by atmospheric fields at their lateral boundaries (pressure, wind, temperature, humidity), at the top of the troposphere (temperature, wind), as well as by sea surface conditions (sea ice concentration, sea surface temperature) every six hours. Consequently, regional atmospheric models add details and physics to the forcing model in the mid and lower troposphere and at the land or iced surface, whereas large-scale circulation patterns are driven by the forcing fields. We forced MAR with three reanalyses over Antarctica in order to evaluate the uncertainty in the simulated surface climate arising from the uncertainty in the assimilation systems: the European Centre for Medium-Range Weather Forecasts "Interim" re-analysis (here-after ERA-Interim, resolution ∼0.75°, i.e. ∼50 km at 70 °S, Dee et al., 2011), the Modern-Era Retrospective analysis for Research and Applications Version 2 (here-after MERRA2, resolution ∼0.5°, Gelaro et al., 2017), and the Japanese 55-year Reanalysis from the Japan Meteorological Agency (here-after JRA-55, resolution ∼1.25°, Kobayashi et al., 2015).

Table 1. Sectors extracted from the GLACIOCLIM-SAMBA database.

Sector name	Sector type	Nb. of obs.	Nb. of grid cells	Year range	Elevation range (m)	Ref.
Ross–Mary Byrd Land (margin)	Scattered	28	26	1955–1994	50–1781	[1,2,3]
Ross–Mary Byrd Land (inland)	Scattered	72	51	1950–1991	37–1995	[1,2,3]
Victoria Land	Scattered	60	40	1951–2006	1804–3240	[4,5,6]
Dumont-d'Urville–Dome C	Transect	116	24	1955–2010	633–3240	[4,7,8,9]
Law Dome–Wilkes Land	Transect	382	32	1973–1986	801–2232	[10]
Zhongshan–Dome A	Transect	583	40	1994–2011	1031–4081	[11,12]
Mawson–Lambert Glacier	Transect	515	36	1990–1995	1883–2924	[13]
Syowa–Dome F	Transect	507	38	1955–2010	584–3803	[14]
Princ. Elisabeth	Transect	58	6	2009–2012	47–1071	[15]
Dronning Maud Land	Scattered	376	104	1955–2008	1753–3741	[16,17,18,19]

[1] Clausen et al. (1979), [2] Venteris and Whillans (1998), [3] Vaughan et al. (1999), [4] Magand et al. (2007), [5] Frezzotti et al. (2004), [6] Frezzotti et al. (2007), [7] Pettré et al. (1986), [8] Agosta et al. (2012), [9] Verfaillie et al. (2012), [10] Goodwin (1988), [11] Ding et al. (2011), [12] Wang et al. (2016), [13] Higham and Craven (1997), [14] Wang et al. (2015), [15] GLACIOCLIM-BELARE, [16] Picciotto et al. (1968), [17] Mosley-Thompson et al. (1995), [18] Mosley-Thompson et al. (1999), [19] Anschütz et al. (2011).

The regional atmospheric model RACMO2 is forced by ERA-Interim. We focus our study to the period 1979-2015, as reanalyses are known to be unreliable before 1979, when satellite sounding data started to be assimilated (Bromwich et al., 2007).

2.2 Observations

2.2.1 SMB observations and sectors of strong SMB gradients

We use surface mass balance observations of the GLACIOCLIM-SAMBA dataset detailed in Favier et al. (2013) and updated by Wang et al. (2016). This dataset is an update of the one assembled by Vaughan et al. (1999) following the quality-control methodology defined by Magand et al. (2007). It includes 3043 reliable SMB values averaged over more than 3 years.

The first order feature of the Antarctic SMB is a strong coastal-inland gradient, with mean values ranging from typically greater than 500 $\mathrm{kg\ m^{-2}\ yr^{-1}}$ at the ice sheet margins to about 30 $\mathrm{kg\ m^{-2}\ yr^{-1}}$ in the dry interior plateau (Fig. 1, see also, e.g., Wang et al., 2016). We divide the sparse observation dataset (Fig. 1 – 5% of MAR grid cells coverage of the ice sheet) into 10 sectors detailed in Table 1 and shown in Fig. 2. Six of them are stake transects with a stake every ∼1.5 km, which have been proven very valuable for evaluating modelled SMB (Agosta et al., 2012; Favier et al., 2013; Wang et al., 2016). The four other sectors are composed of more scattered observations covering large elevation ranges (Victoria Land, Dronning Maud Land, and Ross Ice Shelf–Mary Byrd Land).

2.2.2 Model-observation comparison method

RACMO2 outputs are bi-linearly interpolated to the 35×35 km MAR grid. For each SMB observation, we consider the 4 surrounding MAR grid cells, from which we eliminate ocean grid cells. We also eliminate surrounding grid cells with an elevation difference with the observation greater than 200 m (missing elevation of observation is set to Bedmap2 elevation at 1 km resolution). Finally, we bi-linearly interpolate model values of the remaining grid cells at the observation location (see schematic in Fig. S2).

As we restrict our modelling study to the 1979-2015 period, we only consider observations beginning after 1950. For observations beginning after 1979, we time-average model outputs for the same period as the observation. For observations beginning before 1979, we only consider those covering more than eight years, and we time-average model outputs over the full simulated 1979-2015 period.

In a last step, we average-out the kilometre-scale variability of the observed SMB (Agosta et al., 2012) by binning point values onto grid cells. For each grid cell containing multiple observations, we average all observations contained into the grid cell weighted by the time span of observations, and in the same way we weight-average the modelled values interpolated to observation locations. This way, we obtain consistent observed and modelled averaged values on grid cells.

We discard 66 observations beginning before 1979 and spanning less than eight years. We also discard 12 observations for which the four surrounding grid cells fall in ocean, and seven observations located at specific topographic features for which none of the four surrounding grid cell has an elevation difference less than 200 m with respect to the actual location. After this, we retain 559 model-observation comparisons.

3 Results

3.1 Evaluation of the modelled SMB

The large spatial Antarctic SMB gradients, shown in Fig. 1a as modelled by MAR forced by ERA-Interim for the period 1979-2015, coincide with a strong interannual variability (Fig. 1b), expressed by a standard deviation of ∼22% of the mean SMB on average over the ice sheet (Fig. 1c). MAR SMB oscillates around the 559 observed values (Fig. 1d), with a mean bias of 9 kg m^{-2} yr^{-1} (7% of the mean observed SMB) and a RMSE of 76 kg m^{-2} yr^{-1} (60% of the mean observed SMB).

The model-observation comparison by sectors (Fig. 2) reveals a good representation of the coast-to-plateau SMB gradients by both RCMs. MAR and RACMO2 are in good agreement despite MAR not including drifting snow processes whereas RACMO2 does, except in Ross–Mary Byrd Land and in Victoria Land where MAR simulates larger SMB than RACMO2. Another noticeable result is that MAR forced by ERA-Interim, JRA-55 and MERRA2 give very similar results, not only at the observation locations (Fig. 2) but also at the ice sheet scale (Fig. S4, note the colour map scales compared to Fig. S9). This is why we focus on MAR forced by ERA-Interim in the following.

We find no significant differences in the SMB simulated by MAR and RACMO2 when integrated over the ice sheet or its major basins (Table 2). SMB is driven by snowfall amounts, which are more than 10 times larger than other SMB components.
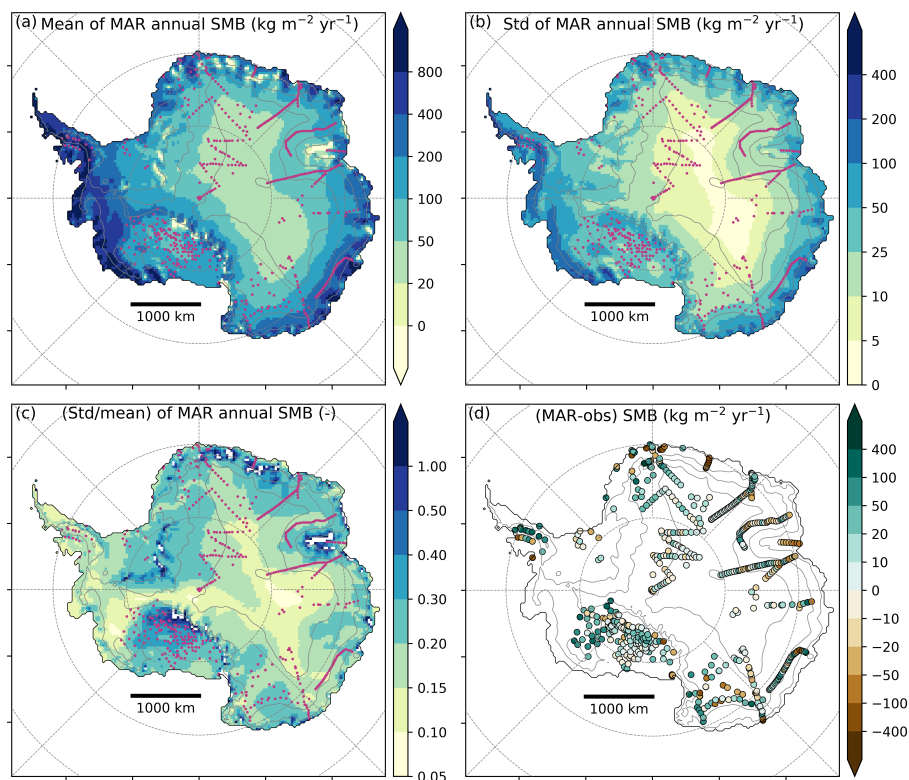
Figure 1. MAR SMB for the period 1979-2015: (a) mean annual SMB (b) standard deviation of annual SMB (c) standard deviation divided by mean annual SMB (d) difference between MAR and observed SMB on MAR grid cells, following the methodology detailed in Section 2.2.2. Solid grey lines are contours of surface height every 1000 m.

Snow sublimation in RACMO2 is the sum of sublimation at the surface of the snowpack and of drifting snow sublimation, and is approximately 50 % larger than in MAR which only includes surface snow sublimation. However, surface snow sublimation alone is almost two times larger in MAR than in RACMO2 (Table 2, also shown in Fig. S5), which we investigate in the next section. Modelled surface melt is less than half of the sublimation amount, however liquid water almost entirely refreezes into the snowpack in both models (maps of modelled melt amounts are shown in Fig. S6). Temporal variability of the SMB and its components is fully driven in both RCMs by the forcing reanalyses and are therefore strongly correlated with each other (time series shown in Fig. S7). We do not elaborate on the SMB temporal variability here as this aspect will be further detailed in a forthcoming study.

3.2 Erosion-deposition features

Oscillations of observed SMB around the smooth modelled SMB gradient are particularly apparent along the four stake transects covering more than 500 km: Law Dome–Wilkes Land, Zhongshan–Dome A, Mawson–Lambert Glacier, and Syowa–
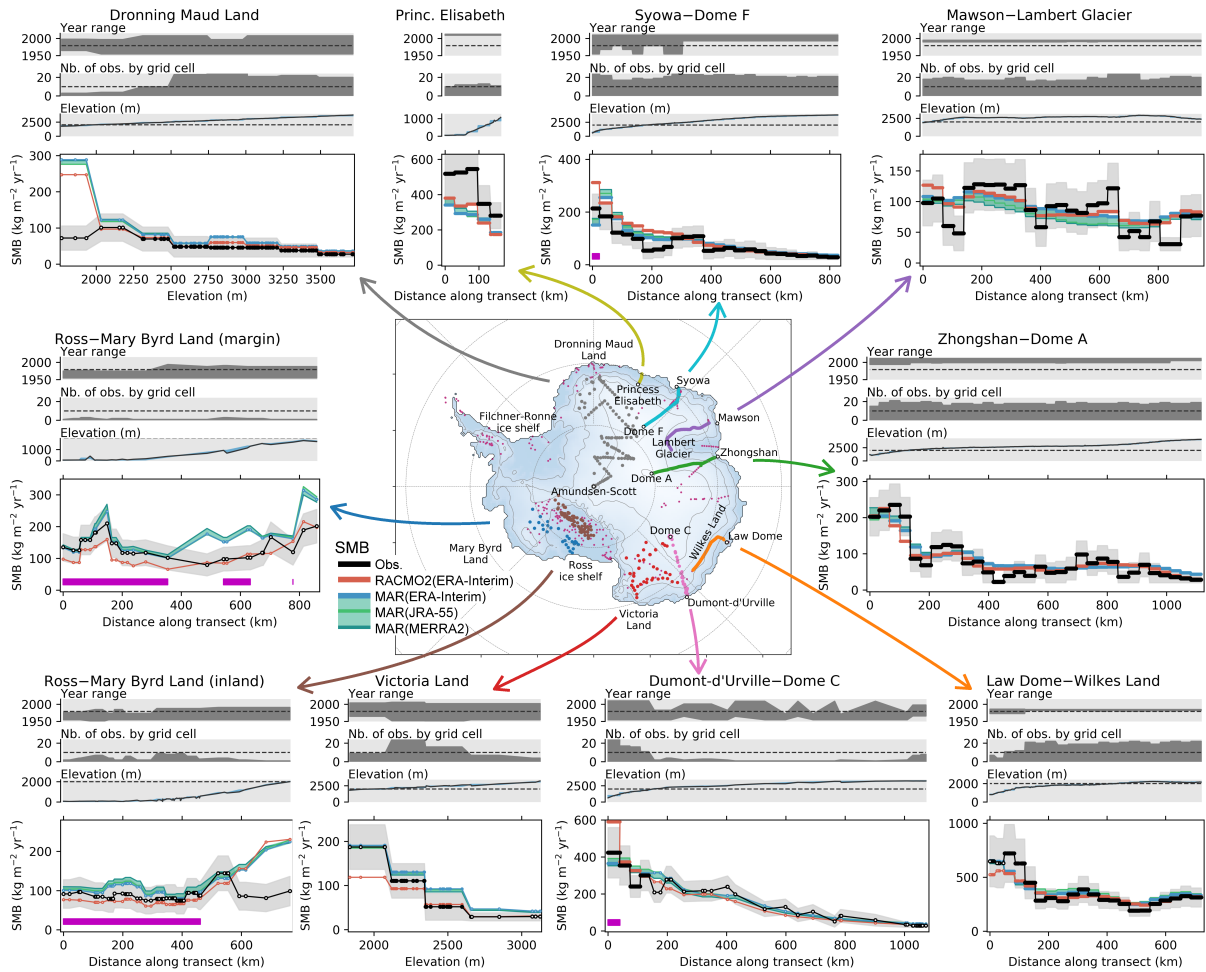
Figure 2. Modelled vs. observed SMB for sectors and transects as detailed in Table 1. RACMO2 outputs are bi-linearly interpolated to the MAR grid. SMB values are first averaged on MAR grid cells (Sec. 2.2.2) then along chosen grid direction (Fig. S2) or by elevation bins. Distance along transect starts at the coast. Uncertainty of observed SMB (grey shaded area) is the standard deviation of observations contained in each grid cell (sub-grid variability), estimated as a function of the mean observed SMB (see Fig. S3). Despite SMB values corresponding to grid cell averages, we display one marker for each observation, with the *x* axis corresponding to the observation location along transect or elevation. Markers with white faces are for bins containing less than 10 observations and black faces for bins containing more than 10 observations. Magenta bands mark grid cells where more than 15 % of precipitation sublimates in the katabatic layers according to Grazioli et al. (2017).

Dome F. As snow is usually eroded from topographic crests and collected in valleys, we computed the surface elevation mean curvature to locate crests (positive curvature, convex surface) and valleys (negative curvature, concave surface) in the MAR

Table 2. Antarctic integrated SMB on average for 1979-2015 $\pm$ one standard deviation of annual values, in Gt yr^{-1}. The upper part of the table is for Total Ice Sheet, with ice shelves (TIS), and the lower part for Grounded Ice Sheet (GIS). Ice sheet and basins geometry are based on Rignot et al., 2017 (in preparation). RACMO2 is bi-linearly interpolated on MAR grid and the same mask is applied to both models, with area given for this mask.

Basin	Area (10^6 km^2)	Component (Gt yr^{-1})	MAR(ERA-Interim)	RACMO2(ERA-Interim)
TIS w/o Peninsula	13.41	SMB	2200 ± 115	2182 ± 107
		Snowfall	2306 ± 111	2339 ± 107
		Rainfall	6 ± 1	2 ± 1
		Surface snow sublimation	111 ± 10	57 ± 4
		Drifting snow sublimation	–	101 ± 5
		Erosion-deposition	–	5 ± 0
		Melt	40 ± 20	68 ± 30
		Run-off	1 ± 1	1 ± 1
TIS	13.83	SMB	2517 ± 111	2525 ± 105
GIS	12.27	SMB	2120 ± 99	2076 ± 93
GIS w/o Peninsula	12.04	SMB	1923 ± 100	1861 ± 94
EAIS	9.77	SMB	1170 ± 89	1120 ± 80
WAIS	2.11	SMB	675 ± 62	645 ± 62
Islands	0.16	SMB	78 ± 7	96 ± 8
Peninsula	0.23	SMB	198 ± 26	214 ± 28

35×35 km elevation grid. In Fig. 3, we notice that both RCMs commonly exhibit an excess of accumulation on crests and a deficit of accumulation in valleys, in the range of ± 40 kg m^{-2} yr^{-1}.

To quantify this curvature effect, we correlate MAR SMB bias (ΔSMB) with the curvature. Curvature is shifted by $\pm$ one grid cell (2 grid cells for Syowa–Dome F) along each transect according to the maximum correlation with ΔSMB (Fig. S8). When

5   the mean annual wind speed (ws_{10}) is greater than seven m s^{-1}, the difference between modelled and observed SMB (in kg m^{-2} yr^{-1}) is scaled to approximately 3700 ± 1100 (in 10^6 kg m^{-1} yr^{-1}) times the curvature (in 10^{-6} m^{-1}), with a significant relationship ($R^2 = 0.43$, Fig. 4a). For lower wind speed ($ws_{10} < 7$ m s^{-1}), we no longer observe any relationship between model bias in SMB and curvature (horizontally aligned squares in Fig. 4a). This is consistent with the erosion deposition process which requires the wind speed to reach threshold values to be initiated (Amory et al., 2015).

10   Hence, a large part of the discrepancies between modelled and observed SMB is explained by elevation curvature when wind speed is sufficiently high, which we relate to the unresolved erosion-deposition process in MAR. Indeed, katabatic winds blowing on the surface of the ice sheet result from the downslope gravity flow of cold, dense air. As a consequence, surface wind speed is related to the slope of the ice sheet: slopes becoming steeper (positive curvature) will lead to wind speed acceleration,
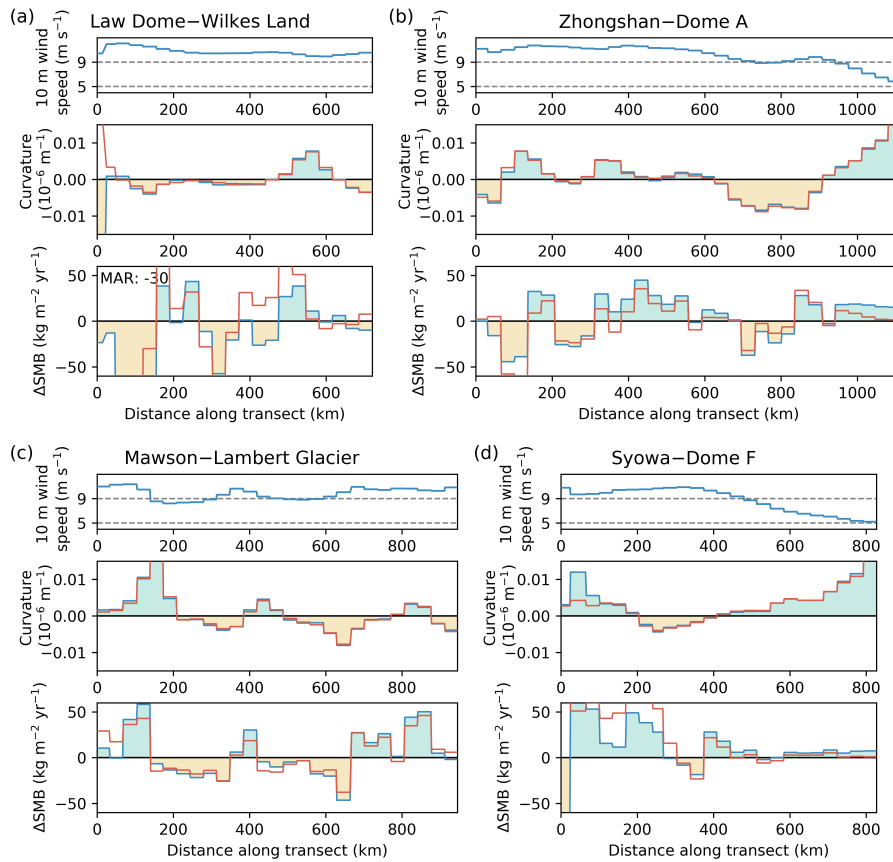
Figure 3. For each transect, we show (top) annual mean 10 m wind speed, (middle) curvature of elevation and (bottom) difference in SMB between models and observation. Blue lines and colour shading are for MAR(ERA-Interim) outputs and red lines are for RACMO2(ERA-Interim) outputs. Values are computed as in Fig. 2. For Law Dome–Wilkes Land, MAR SMB is shifted by -30 kg m^{-2} yr^{-1}.

thus to mass export, whereas slopes becoming more gentle (negative curvature) will lead to wind speed deceleration, thus to mass deposit.

In Figure 4b, we propose a spatial estimate of the erosion-deposition fluxes not resolved by MAR, computed as a simple function of curvature and wind speed as described above. This estimate turns out to be remarkably comparable to the erosion-deposition pattern modelled by RACMO2 (Fig. 4c), except that it gives fluxes approximately three times larger than in RACMO2 (see differences in colour map scales between Fig. 4b and 4c, fluxes summed over the ice sheet and associated uncertainties are detailed in Table S2).

The erosion-deposition estimate consists in a redistribution of mass with negligible net mass loss over the Antarctic ice sheet (total AIS erosion of $\sim$80 Gt yr^{-1} and total AIS deposition of $\sim$75 Gt yr^{-1}, see Table S2). It can be interpreted as the transport of suspended snow particles after sublimation in the atmospheric boundary layer, similarly to how erosion-deposition is modelled in RACMO2. Missing drifting snow sublimation in MAR is generally compensated by stronger sublimation at
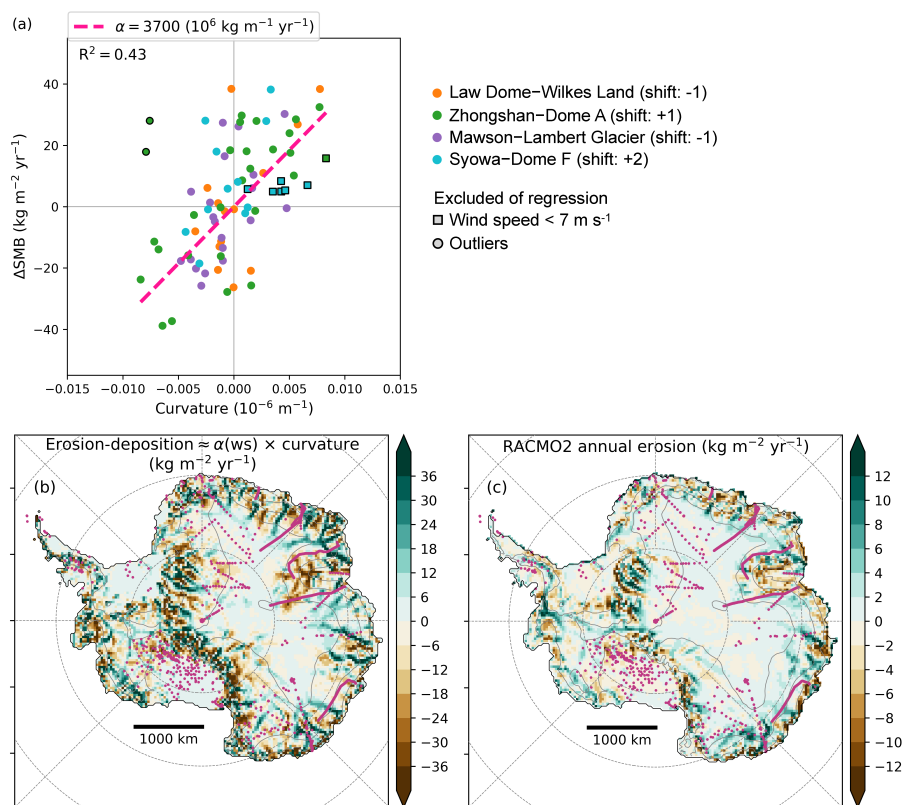
Figure 4. (a) Difference in SMB by grid cell (ΔSMB) between MAR(ERA-Interim) and observations for four transects (Law Dome–Wilkes Land, Zhongshan–Dome A, Mawson–Lambert Glacier, and Syowa–Dome F) vs. elevation curvature on MAR grid. Curvature is shifted by $\pm$ 1–2 grid cells according to the maximum correlation with ΔSMB (Fig. S8). Linear regression through the origin is plotted with a dashed pink line. We excluded of regression two outliers (dots with black contour) and seven data for which MAR annual 10 m wind speed is lower than 7 m s^{-1} (squares with black contour). (b) Estimate of mean annual erosion-deposition based on a scaling of the curvature: erosion-deposition (kg m^{-2} yr^{-1}) = α (10^6 kg m^{-1} yr^{-1}) $\times$ curvature (10^{-6} m^{-1}), with $\alpha = 0$ kg m^{-1} yr^{-1} for wind speed lower than 5 m s^{-1}, $\alpha = 3700$ 10^6 kg m^{-1} yr^{-1} for wind speed greater than 9 m s^{-1}, and α linearly increasing as a function of wind speed in between. Wind speed is the annual mean of 10 m wind speed modelled by MAR(ERA-Interim). (c) Mean annual erosion-deposition flux in RACMO2 on average for 1979-2015 (kg m^{-2} yr^{-1}).

the surface of the snowpack than in RACMO2 (Table 2 and Fig. S5), mainly because of dryer atmospheric layers in MAR. However, drifting snow sublimation is a potentially larger mass sink than surface snow sublimation, as drifting snow particles are continuously ventilated and fully exposed to the ambient air, even though this process is bounded by the water vapour holding capacity of the atmosphere (Bintanja, 2001). Consequently, by accounting for drifting snow in MAR we expect that

5 the drifting snow sublimation mass sink could be enhanced at the expense of surface snow sublimation, at least in areas where surface wind speed is high and the atmospheric boundary layer is strongly undersaturated.
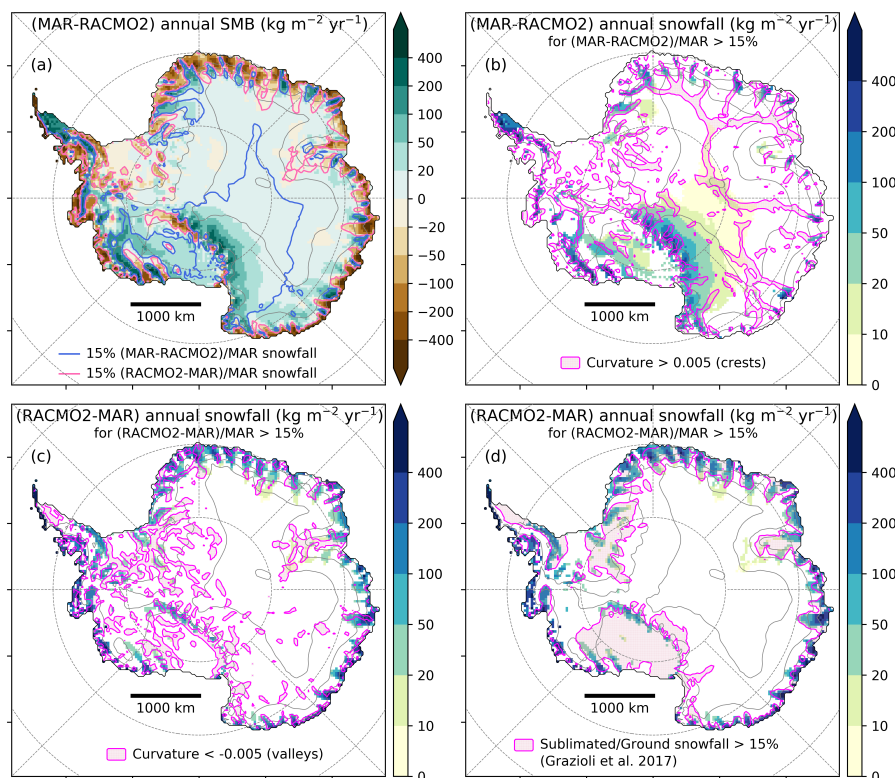
Figure 5. The four maps show mass fluxes in $\mathrm{kg\ m^{-2}\ yr^{-1}}$ on average for the period 1979-2015. (a) Difference in SMB between MAR and RACMO2. Solid blue lines delimitate areas where MAR snowfall is greater than RACMO2 snowfall by more than 15 % and solid pink lines areas where RACMO2 snowfall is greater than MAR snowfall by more than 15 %. (b) Difference in snowfall between MAR and RACMO2 when MAR snowfall is greater than RACMO2 snowfall by more than 15 %. Pink shading shows areas where curvature is greater than 0.005 (crests). (c) Difference in snowfall between RACMO2 and MAR when RACMO2 snowfall is greater than MAR snowfall by more than 15 %. Pink shading shows areas where curvature is lower than -0.005 (valleys). (d) Same as (c) but with pink shading in areas where sublimation of precipitation in the low-level atmospheric layers is greater than 15 % of ground precipitation as estimated by Grazioli et al. (2017) for the year 2015.

3.3 Sublimation of precipitation in katabatic channels

As described above, the dynamical downscaling of ERA-Interim with RACMO2 and MAR results in similar spatial patterns for SMB as compared to observations. However, at the ice sheet scale, MAR and RACMO2 show regional discrepancies (Figure 5a) which are primarily the result of differences in simulated snowfall rates (Fig. S9). In this section we focus on areas where RACMO2 snowfall is greater than MAR snowfall by more than 15 %. Those areas are generally located on the east side of valleys (curvatures < -0.005, Fig. 5c). We relate this to the recent work of Grazioli et al. (2017) which demonstrates that precipitation sublimates in katabatic channels at the ice sheet margins. This is because surface air flux, moving from

high-elevated inland plateau toward sea level, is subject to adiabatic compression when it moves downslope. This compression induces an increase in air temperature which reduces relative humidity and drives sublimation rates. We find that areas of low-level sublimation derived from observations and modelling in Grazioli et al. (2017) coincide almost exactly with areas where MAR snowfall is much lower than RACMO2 snowfall (Fig. 5d). In MAR precipitating particles are explicitly advected

5   through the atmospheric layers until they reach the surface, thus enabled to sublimate in the undersaturated katabatic layers, while in RACMO2 precipitation is added to the surface without advection/sublimation through the atmosphere.

We conclude, as in Grazioli et al. (2017), that low-level sublimation is an important process at the ice sheet margins, as for the period 1979-2015 it may represent $\sim$240$\pm$25 Gt yr^{-1} of difference in snowfall between RACMO2 and MAR (summed on areas where RACMO2 snowfall is greater than MAR snowfall by more than 15%, Peninsula excluded, $\pm$ interannual

10   variability). This value represents 10 % of the total MAR snowfall loaded over the ice sheet (Table 2), and 20 % for areas under 1000 m above sea level (asl). We obtain the same quantity for the year 2015, when the amount of snowfall never reaching the ground has been estimated by Grazioli et al. (2017) to be of 240 $\pm$ 40 Gt yr^{-1}, after interpolation on the MAR grid and for areas where sublimation is greater than ground precipitation by more than 15%, with uncertainty computed by moving this ratio between 10% and 20%.

15   It is noticeable that very few SMB observations are available in areas where Grazioli et al. (2017) identify low-level sublimation, marked by magenta bands in Fig. 2. Except for Ross–Mary Byrd Land, the only other areas where low-level sublimation is greater than 15 % of the total precipitation as defined by Grazioli et al. (2017) are close to Dumont d'Urville (coastal Adelie Land) and to Syowa (coastal Dronning Maud Land). In those areas the SMB amount is indeed larger in RACMO2 than in MAR and in observations. Both RCMs overestimate SMB around 2000 m in Dronning Maud Land and in Mary Byrd Land (Fig. 2),

20   which could indicate katabatic channels not enough resolved by the topography of the models.

3.4   SMB overestimation in MAR and wind glaze areas

MAR simulates significantly larger snowfall amounts than RACMO2 (>15 %) in areas centred on crests under 2000 m asl (Fig. 5b, curvature > 0.005). Those locations are the topographic counterparts of katabatic channels outlined in the previous section, where RACMO2 snowfall is larger than MAR snowfall likely because of missing low-level sublimation of precipi-

25   tation. MAR also simulates larger snowfall than RACMO2 on the inland plateau. Observations do not enable to definitively discriminate one model against the other, but we observe a general tendency for MAR to overestimate accumulation on the Ross side of Mary Byrd Land and close to ice sheet summits (Dome C, Dome A, Dome F, see Fig. 1d and Fig. 2). Close to summits the wind is low, so missing erosion-deposition process is unlikely explanation for a positive bias in SMB modelled by MAR (Fig. 4c). Over the Greenland ice sheet, MAR tends to overestimate ice cores based accumulation inland (Fettweis et al.,

30   2017) while RACMO2 underestimates it (Noël et al., 2018).

The larger snowfall amount in MAR than in RACMO2 is particularly significant south of Victoria Land, on the lee side of the Transantarctic Mountains. Simulated snowfall rates in this region are potentially sensitive to cloud microphysics (Fig. 3a of van Wessem et al., 2017), to model resolution via orographic precipitation and foehn effect (27 km in RACMO2 vs 35 km in MAR), and to local circulation near the mountains. In this region, we find four grid cells where MAR SMB is significantly

larger than observed SMB (Fig. 1d), which tends to confirm a SMB overestimation in MAR even if those data are composed of point observations possibly not capturing the spatial heterogeneity over 35 km grid cell areas. Interestingly, this unobserved area where MAR simulates larger snowfall amounts than RACMO2 is classified as a large wind glaze area in Scambos et al. (2012, see their Fig. 9). In their study, Scambos et al. (2012) outlined that those wind glaze areas could arise from eroded snow

5 sublimating in the undersaturated katabatic layer. This would result in a net mass loss for the ice sheet, as surface snow is moved to suspended snow by the erosion process, then to water vapour by the low-level sublimation process, and subsequently exported outside the ice sheet by the katabatic flow.

4 Discussion and conclusion

In our study, we evaluate new estimates of the Antarctic SMB obtained with the polar RCM MAR run for the first time for

10 decades-long simulations at the scale of the whole Antarctic ice sheet. We use model settings comparable to previous MAR simulations over Greenland (Fettweis et al., 2017) but with a specific upper atmosphere relaxation and new fresh snow density and roughness length parameterisations. We present the dynamical downscaling of ERA-Interim, JRA-55 and MERRA2 with MAR for the satellite era (1979-2015) where we can rely on reanalyses products. Remarkably, MAR forced by those three reanalyses give similar spatial and temporal SMB patterns. We also compare MAR with the latest simulations of the RCM

15 RACMO2 forced by ERA-Interim (van Wessem et al., 2017). We find no significant differences between MAR and RACMO2 SMB when integrated on the AIS and its major basins (Table 2).

As the dominant feature of the Antarctic SMB is its strong coast to plateau gradient, we extract stake transects and sectors with large elevation ranges from the GLACIOCLIM-SAMBA SMB observational dataset. We show that both RCMs show similar performances when compared to observations, with a good representation of the SMB gradient (Fig. 2). But more

20 importantly, we outline and quantify missing processes in both RCMs.

Along stake transects, we relate 100 km-scale oscillations of observations around the smooth modelled SMB pattern to the shape of the ice sheet captured on the 35×35 km MAR grid. Both RCMs accumulate too much snow on crests, and not enough snow in valleys, as a result of erosion-deposition processes not included in MAR and probably underestimated in RACMO2 by a factor of three (Fig. 4). The RACMO2 snowdrift routine separately estimates sublimation of eroded snow and

25 erosion-deposition, the latter being achieved as redistribution of the mass without mass change. In MAR, the missing snowdrift sublimation process is compensated by higher sublimation rates at the surface of the snowpack compared to RACMO2 (Table 2) driven by dryer surface atmospheric layers in MAR. Widespread wind glaze areas as described in Scambos et al. (2012), formed by the sublimation of eroded snow in the boundary layer, are resolved neither by MAR nor by RACMO2. This is likely because our MAR simulations do not resolve the drifting snow (despite a drifting snow module exists into MAR, e.g. Amory et al.,

30 2015) and RACMO2 potentially underestimates drifting snow fluxes.

We also point out that MAR generally simulates larger SMB and snowfall amounts than RACMO2, except in areas where precipitation sublimates while falling through the undersaturated katabatic layer as identified by Grazioli et al. (2017). As precipitating snow particles are not advected through the atmospheric layers in RACMO2 as it is in MAR, the mass difference

in areas where MAR snowfall is significantly lower than RACMO2 snowfall can be interpreted as precipitation lost by low-level sublimation in katabatic channels. This amount represents $\sim$240±25 Gt yr^{-1} over the ice sheet (Peninsula excluded), which is more than twice the surface snow sublimation (Table 2), 97 % of which is lost below 2000 m asl, and 78 % below 1000 m asl. This might be of importance for the mass balance of glacier drainage basins (SMB minus discharge, Rignot

5   et al., 2008; Shepherd et al., 2012), as ice streams are typically channel-shaped areas affected by low-level sublimation of precipitation. Consequently, we note the importance of saving precipitation fluxes in models at least 1300 m above the ground for comparison with CloudSat products, but ideally at all model levels below 1500 m above the ground to be able to compute sublimation of precipitation in the low-level atmospheric layers. This was not the case for MAR and RACMO2 outputs used in this study, but it will become a standard output in forthcoming MAR simulations.

10   We expect that accounting for drifting snow in MAR will lead to significant improvements in describing the Antarctic SMB and surface climate, as it will enable (1) a quantification of the drifting snow sublimation mass sink, (2) a more realistic representation of relative humidity and temperature in the boundary layer, and (3) an explicit modelling of near-zero accumulation areas (wind glaze areas) and of the redistribution of snow from crests to valleys. Exploring the impact of horizontal and vertical model resolution on drifting snow estimates and on sublimation of precipitation in katabatic channels will also be of importance

15   as those processes are related to the shape of the ice sheet.

Code and data availability. Python scripts developed for this study as well as all required data are available at https://gitlab.com/cecileagosta/antarctica-smb-20c.git. The last version of MAR is freely distributed at http://mar.cnrs.fr/. Monthly MARv3.6.4 outputs from this study are freely available at ftp://ftp.climato.be/fettweis/MARv3.6/Antarctic/, together with the associated MAR source code. The ECMWF reanalyse ERA-Interim 6-hourly outputs were downloaded from http://apps.ecmwf.int/datasets/. The MERRA2 reanalyse 6-hourly outputs were downloaded

20   from https://disc.sci.gsfc.nasa.gov/. The JRA-55 reanalyse 6-hourly outputs were downloaded from https://rda.ucar.edu/datasets/ds628.0/.

Author contributions. Cécile Agosta set-up the MAR model for Antarctica with several adaptations, performed model simulations and analysed model outputs and observations. Cécile Agosta, Anais Orsi, Xavier Fettweis and Vincent Favier designed the study. Cécile Agosta, Xavier Fettweis, Hubert Gallée, Charles Amory and Christoph Kittel developed the MAR model and contributed to the MAR set-up and output analyses. Xavier Fettweis and Hubert Gallée are the main developer of the MAR model. Michiel R. van den Broeke, J. Melchior van

25   Wessem and Jan Lenaerts contributed to RACMO2 output analyses. All authors contributed to discussions in writing this manuscript.

Competing interests. The authors declare that they have no conflict of interests.

Acknowledgements. Cécile Agosta is a postdoctoral research fellow of the Belgian National Fund for Scientific Research (FRS-FNRS). Computational resources have been provided by the Consortium des Équipements de Calcul Intensif (CÉCI), funded by the Fonds de la

Recherche Scientifique de Belgique (F.R.S.-FNRS) under Grant No. 2.5020.11. We acknowledge Jacopo Grazioli for sharing low-level sublimation product and his expertise of this dataset. We acknowledge Yetang Wang for sharing his updated version of the GLACIOCLIM-SAMBA dataset. We acknowledge Christophe Genthon for fruitful discussions and suggestions. The authors acknowledge the support from Agence Nationale de la Recherche scientific for the scientific traverses in Antarctica and the associated research on climate and surface mass

5   balance modeling, projects ANR-14-CE01-0001 (ASUMA) and ANR-16-CE01-0011 (EAIIST).

References

Agosta, C., Favier, V., Genthon, C., Gallée, H., Krinner, G., Lenaerts, J. T., and van den Broeke, M. R.: A 40-year accumulation dataset for Adelie Land, Antarctica and its application for model validation, Climate Dynamics, 38, 75–86, https://doi.org/10.1007/s00382-011-1103-4, http://link.springer.com/article/10.1007/s00382-011-1103-4/fulltext.html, 2012.

5 Amory, C., Trouvillez, A., Gallée, H., Favier, V., Naaim-Bouvet, F., Genthon, C., Agosta, C., Piard, L., and Bellot, H.: Comparison between observed and simulated aeolian snow mass fluxes in Adélie Land, East Antarctica, The Cryosphere, 9, 1373–1383, https://doi.org/10.5194/tc-9-1373-2015, http://www.the-cryosphere.net/9/1373/2015/, 2015.

Amory, C., Gallée, H., Naaim-Bouvet, F., Favier, V., Vignon, E., Picard, G., Trouvillez, A., Piard, L., Genthon, C., and Bellot, H.: Seasonal Variations in Drag Coefficient over a Sastrugi-Covered Snowfield in Coastal East Antarctica, Boundary-Layer Meteorology, 164, 107–133,
10 https://doi.org/10.1007/s10546-017-0242-5, https://link.springer.com/article/10.1007/s10546-017-0242-5, 2017.

Anschütz, H., Sinisalo, A., Isaksson, E., McConnell, J. R., Hamran, S. E., Bisiaux, M. M., Pasteris, D., Neumann, T. A., and Winther, J.-G.: Variation of accumulation rates over the last eight centuries on the East Antarctic Plateau derived from volcanic signals in ice cores, Journal of Geophysical Research: Atmospheres (1984–2012), 116, 456, https://doi.org/10.1029/2011JD015753, https://agupubs.onlinelibrary.wiley.com/doi/full/10.1029/2011JD015753, 2011.

15 Arthern, R. J., Winebrenner, D. P., and Vaughan, D. G.: Antarctic snow accumulation mapped using polarization of 4.3-cm wavelength microwave emission, Journal of Geophysical Research: Atmospheres (1984–2012), 111, 249, https://doi.org/10.1029/2004JD005667, http://onlinelibrary.wiley.com/doi/10.1029/2004JD005667/full, 2006.

Bintanja, R.: Modelling snowdrift sublimation and its effect on the moisture budget of the atmospheric boundary layer, Tellus A: Dynamic Meteorology and Oceanography, 53, 215–232, 2001.

20 Bromwich, D. H., Fogt, R. L., Hodges, K. I., and Walsh, J. E.: A tropospheric assessment of the ERA-40, NCEP, and JRA-25 global reanalyses in the polar regions, Journal of Geophysical Research: Atmospheres (1984–2012), 112, D10 111, https://doi.org/10.1029/2006JD007859, http://onlinelibrary.wiley.com/doi/10.1029/2006JD007859/full, 2007.

Brun, E., David, P., Sudul, M., and Brunot, G.: A numerical model to simulate snow-cover stratigraphy for operational avalanche forecasting, Journal of Glaciology, 38, 13–22, https://doi.org/10.3189/S0022143000009552, https://www.cambridge.org/core/product/identifier/
25 S0022143000009552/type/journal_article, 1992.

Clausen, H. B., Dansgaard, W., Nielsen, J., and Clough, J. W.: Surface accumulation on Ross Ice Shelf, Antarctic Journal of the United States, 14, 68–72, 1979.

De Ridder, K. and Gallée, H.: Land Surface–Induced Regional Climate Change in Southern Israel, Journal of Applied Meteorology, 37, 1470–1485, https://doi.org/10.1175/1520-0450(1998)037<1470:LSIRCC>2.0.CO;2, https://journals.ametsoc.org/doi/abs/10.1175/1520-0450%
30 281998%29037%3C1470%3ALSIRCC%3E2.0.CO%3B2, 1998.

Dee, D. P., Uppala, S. M., Simmons, A. J., Berrisford, P., Poli, P., Kobayashi, S., Andrae, U., Balmaseda, M. A., Balsamo, G., Bauer, P., Bechtold, P., Beljaars, A. C. M., van de Berg, L., Bidlot, J., Bormann, N., Delsol, C., Dragani, R., Fuentes, M., Geer, A. J., Haimberger, L., Healy, S. B., Hersbach, H., Hólm, E. V., Isaksen, L., Kållberg, P., Köhler, M., Matricardi, M., McNally, A. P., Monge Sanz, B. M., Morcrette, J. J., Park, B. K., Peubey, C., de Rosnay, P., Tavolato, C., Thépaut, J. N., and Vitart, F.: The ERA-Interim reanalysis:
35 configuration and performance of the data assimilation system, Quarterly Journal of the Royal Meteorological Society, 137, 553–597, https://doi.org/10.1002/qj.828, http://onlinelibrary.wiley.com/doi/10.1002/qj.828/full, 2011.

Ding, M., Xiao, C., Li, Y., Ren, J., Hou, S., Jin, B., and Sun, B.: Spatial variability of surface mass balance along a traverse route from Zhongshan station to Dome A, Antarctica, Journal of Glaciology, 57, 658–666, https://doi.org/10.3189/002214311797409820, http://www.ingentaconnect.com/content/igsoc/jog/2011/00000057/00000204/art00008, 2011.

Eisen, O., Frezzotti, M., Genthon, C., Isaksson, E., Magand, O., van den Broeke, M. R., Dixon, D. A., Ekaykin, A., Holmlund, P., Kameda, T., Karlof, L., Kaspari, S., Lipenkov, V. Y., Oerter, H., Takahashi, S., and Vaughan, D. G.: Ground-based measurements of spatial and temporal variability of snow accumulation in East Antarctica, Reviews of Geophysics, 46, 26 367, https://doi.org/10.1029/2006RG000218, http://onlinelibrary.wiley.com/doi/10.1029/2006RG000218/full, 2008.

Ettema, J., van den Broeke, M. R., Meijgaard, E. v., van de Berg, W. J., Box, J. E., and Steffen, K.: Climate of the Greenland ice sheet using a high-resolution climate model – Part 1: Evaluation, The Cryosphere, 4, 511–527, https://doi.org/10.5194/tc-4-511-2010, http://www.the-cryosphere.net/4/511/2010/, 2010.

Favier, V., Agosta, C., Parouty, S., Durand, G., Delaygue, G., Gallée, H., Drouet, A.-S., Trouvillez, A., and Krinner, G.: An updated and quality controlled surface mass balance dataset for Antarctica, The Cryosphere, 7, 583–597, https://doi.org/10.5194/tc-7-583-2013, http://www.the-cryosphere.net/7/583/2013/tc-7-583-2013.html, 2013.

Favier, V., Krinner, G., Amory, C., Gallée, H., Beaumet, J., and Agosta, C.: Antarctica-Regional Climate and Surface Mass Budget, Current Climate Change Reports, pp. 1–13, https://doi.org/10.1007/s40641-017-0072-z, https://link.springer.com/article/10.1007/s40641-017-0072-z, 2017.

Fettweis, X., Franco, B., Tedesco, M., van Angelen, J. H., Lenaerts, J. T., van den Broeke, M. R., and Gallée, H.: Estimating Greenland ice sheet surface mass balance contribution to future sea level rise using the regional atmospheric climate model MAR, The Cryosphere, 7, 469–489, https://doi.org/10.5194/tc-7-469-2013, http://www.the-cryosphere.net/7/469/2013/tc-7-469-2013.html, 2013.

Fettweis, X., Box, J. E., Agosta, C., Amory, C., Kittel, C., Lang, C., As, D. v., Machguth, H., and Gallée, H.: Reconstructions of the 1900–2015 Greenland ice sheet surface mass balance using the regional climate MAR model, The Cryosphere, 11, 1015–1033, https://doi.org/10.5194/tc-11-1015-2017, www.the-cryosphere.net/11/1015/2017/, 2017.

Fretwell, P., Pritchard, H. D., Vaughan, D. G., Bamber, J. L., Barrand, N. E., Bell, R. E., Bianchi, C., Bingham, R. G., Blankenship, D. D., Casassa, G., Catania, G., Callens, D., Conway, H., Cook, A. J., Corr, H. F. J., Damaske, D., Damm, V., Ferraccioli, F., Forsberg, R., Fujita, S., Gim, Y., Gogineni, P., Griggs, J. A., Hindmarsh, R. C. A., Holmlund, P., Holt, J. W., Jacobel, R. W., Jenkins, A., Jokat, W., Jordan, T., King, E. C., Kohler, J., Krabill, W., Riger-Kusk, M., Langley, K. A., Leitchenkov, G., Leuschen, C., Luyendyk, B. P., Matsuoka, K., Mouginot, J., Nitsche, F. O., Nogi, Y., Nost, O. A., Popov, S. V., Rignot, E., Rippin, D. M., Rivera, A., Roberts, J., Ross, N., Siegert, M. J., Smith, A. M., Steinhage, D., Studinger, M., Sun, B., Tinto, B. K., Welch, B. C., Wilson, D., Young, D. A., Xiangbin, C., and Zirizzotti, A.: Bedmap2: improved ice bed, surface and thickness datasets for Antarctica, The Cryosphere, 7, 375–393, https://doi.org/10.5194/tc-7-375-2013, http://www.the-cryosphere.net/7/375/2013/, 2013.

Frezzotti, M., Pourchet, M., Flora, O., Gandolfi, S., Gay, M., Urbini, S., Vincent, C., Becagli, S., Gragnani, R., Proposito, M., Severi, M., Traversi, R., Udisti, R., and Fily, M.: New estimations of precipitation and surface sublimation in East Antarctica from snow accumulation measurements, Climate Dynamics, 23, 803–813, https://doi.org/10.1007/s00382-004-0462-5, https://link.springer.com/article/10.1007/s00382-004-0462-5, 2004.

Frezzotti, M., Urbini, S., Proposito, M., Scarchilli, C., and Gandolfi, S.: Spatial and temporal variability of surface mass balance near Talos Dome, East Antarctica, Journal of Geophysical Research: Atmospheres (1984–2012), 112, 195, https://doi.org/10.1029/2006JF000638, https://agupubs.onlinelibrary.wiley.com/doi/full/10.1029/2006JF000638, 2007.

Gallée, H.: Simulation of the Mesocyclonic Activity in the Ross Sea, Antarctica, Monthly Weather Review, 123, 2051–2069, https://doi.org/10.1175/1520-0493(1995)123<2051:SOTMAI>2.0.CO;2, https://journals.ametsoc.org/doi/abs/10.1175/1520-0493% 281995%29123%3C2051%3ASOTMAI%3E2.0.CO%3B2, 1995.

Gallée, H. and Gorodetskaya, I. V.: Validation of a limited area model over Dome C, Antarctic Plateau, during winter, Climate Dynamics,
5   34, 61, https://doi.org/10.1007/s00382-008-0499-y, https://link.springer.com/article/10.1007/s00382-008-0499-y, 2010.

Gallée, H. and Schayes, G.: Development of a Three-Dimensional Meso-γ Primitive Equation Model: Katabatic Winds Simulation in the Area of Terra Nova Bay, Antarctica, Monthly Weather Review, 122, 671–685, https://doi.org/10.1175/1520-0493(1994)122<0671:DOATDM>2.0.CO;2, https://journals.ametsoc.org/doi/abs/10.1175/1520-0493(1994)122%3C0671:DOATDM% 3E2.0.CO;2, 1994.

10 Gallée, H., Trouvillez, A., Agosta, C., Genthon, C., Favier, V., and Naaim-Bouvet, F.: Transport of snow by the wind: a comparison between Observations in Adélie Land, Antarctica, and Simulations made with the Regional Climate Model MAR, Boundary-Layer Meteorology, 146, 133–147, https://doi.org/10.1007/s10546-012-9764-z, http://link.springer.com/article/10.1007/s10546-012-9764-z, 2013.

Gallée, H., Preunkert, S., Argentini, S., Frey, M. M., Genthon, C., Jourdain, B., Pietroni, I., Casasanta, G., Barral, H., Vignon, E., Amory, C., and Legrand, M.: Characterization of the boundary layer at Dome C (East Antarctica) during the OPALE summer campaign, Atmospheric
15   Chemistry and Physics, 15, 6225–6236, https://doi.org/10.5194/acp-15-6225-2015, http://www.atmos-chem-phys.net/15/6225/2015/, 2015.

Gardner, A. S., Moholdt, G., Scambos, T. A., Fahnstock, M., Ligtenberg, S., Broeke, M. v. d., and Nilsson, J.: Increased West Antarctic and unchanged East Antarctic ice discharge over the last 7 years, The Cryosphere, 12, 521–547, https://www.the-cryosphere.net/12/521/2018/, 2018.

20 Gelaro, R., McCarty, W., Suarez, M. J., Todling, R., Molod, A., Takacs, L., Randles, C. A., Darmenov, A., Bosilovich, M. G., Reichle, R., Wargan, K., Coy, L., Cullather, R., Draper, C., Akella, S., Buchard, V., Conaty, A., da Silva, A. M., Gu, W., Kim, G.-K., Koster, R., Lucchesi, R., Merkova, D., Nielsen, J. E., Partyka, G., Pawson, S., Putman, W., Rienecker, M., Schubert, S. D., Sienkiewicz, M., and Zhao, B.: The Modern-Era Retrospective Analysis for Research and Applications, Version 2 (MERRA-2), Journal of Climate, 30, 5419–5454, https://doi.org/10.1175/JCLI-D-16-0758.1, http://journals.ametsoc.org/doi/10.1175/JCLI-D-16-0758.1, 2017.

25 Genthon, C., Magand, O., Krinner, G., and Fily, M.: Do climate models underestimate snow accumulation on the Antarctic plateau? A re-evaluation of/from in situ observations in East Wilkes and Victoria Lands, Annals of Glaciology, 50, 61–65, https://doi.org/10.3189/172756409787769735, https://www.cambridge.org/core/product/identifier/S0260305500251458/type/ journal_article, 2009.

Goodwin, I.: Ice sheet topography and surface characteristics in eastern Wilkes Land, East Antarctica, p. 100, ANARE research notes,
30   https://books.google.com/books/about/Ice_sheet_topography_and_surface_charact.html?hl=fr&id=SatQAAAAYAAJ, 1988.

Grazioli, J., Madeleine, J.-B., Gallée, H., Forbes, R. M., Genthon, C., Krinner, G., and Berne, A.: Katabatic winds diminish precipitation contribution to the Antarctic ice mass balance., Proceedings of the National Academy of Sciences of the United States of America, 114, 10 858–10 863, https://doi.org/10.1073/pnas.1707633114, http://www.pnas.org/content/114/41/10858.full, 2017.

Higham, M. and Craven, M.: Surface mass balance and snow surface properties from the Lambert Glacier Basin traverses 1990-94, Tech.
35   rep., https://trove.nla.gov.au/version/27325424, 1997.

Kobayashi, S., Ota, Y., Harada, Y., Ebita, A., Moriya, M., Onoda, H., Onogi, K., Kamahori, H., Kobayashi, K., Endo, H., Miyaoka, K., and Takahashi, K.: The JRA-55 Reanalysis: General Specifications and Basic Characteristics, Journal of the Meteorological Society of Japan, 93, 5–48, https://doi.org/10.2151/jmsj.2015-001, https://www.jstage.jst.go.jp/article/jmsj/93/1/93_2015-001/_article, 2015.

Kuipers Munneke, P., van den Broeke, M. R., Lenaerts, J. T., Flanner, M. G., Gardner, A. S., and van de Berg, W. J.: A new albedo parameterization for use in climate models over the Antarctic ice sheet, Journal of Geophysical Research: Atmospheres (1984–2012), 116, F04 018, https://doi.org/10.1029/2010JD015113, http://onlinelibrary.wiley.com/doi/10.1029/2010JD015113/full, 2011.

Lang, C., Fettweis, X., and Erpicum, M.: Future projections of the climate and surface mass balance of Svalbard with the regional climate model MAR, The Cryosphere, 9, 945–956, https://doi.org/10.5194/tcd-9-115-2015, http://www.the-cryosphere.net/9/945/2015/tc-9-945-2015.html, 2015.

Lenaerts, J. T., van den Broeke, M. R., Déry, S., van Meijgaard, E., van de Berg, W. J., Palm, S. P., and Rodrigo, J.: Modeling drifting snow in Antarctica with a regional climate model: 1. Methods and model evaluation, Journal of Geophysical Research, 117, D05 108, https://doi.org/10.1029/2011JD016145, http://www.agu.org/pubs/crossref/2012/2011JD016145.shtml, 2012a.

Lenaerts, J. T., van den Broeke, M. R., van de Berg, W. J., van Meijgaard, E., and Munneke, P.: A new, high-resolution surface mass balance map of Antarctica (1979–2010) based on regional atmospheric climate modeling, Geophysical Research Letters, 39, L04 501, https://doi.org/10.1029/2011GL050713, http://www.agu.org/pubs/crossref/2012/2011GL050713.shtml, 2012b.

Magand, O., Genthon, C., Fily, M., Krinner, G., Picard, G., Frezzotti, M., and Ekaykin, A. A.: An up-to-date quality-controlled surface mass balance data set for the 90°–180°E Antarctica sector and 1950–2005 period, Journal of Geophysical Research, 112, 1, https://doi.org/10.1029/2006JD007691, http://doi.wiley.com/10.1029/2006JD007691, 2007.

Magand, O., Picard, G., Brucker, L., Fily, M., and Genthon, C.: Snow melting bias in microwave mapping of Antarctic snow accumulation, The Cryosphere, 2, 109–115, https://doi.org/10.5194/tc-2-109-2008, http://www.the-cryosphere.net/2/109/2008/, 2008.

Morcrette, J.-J.: Assessment of the ECMWF Model Cloudiness and Surface Radiation Fields at the ARM SGP Site, Monthly Weather Review, 130, 257–277, https://doi.org/10.1175/1520-0493(2002)130<0257:AOTEMC>2.0.CO;2, https://journals.ametsoc.org/doi/full/10.1175/1520-0493%282002%29130%3C0257%3AAOTEMC%3E2.0.CO%3B2, 2002.

Mosley-Thompson, E., Thompson, L. G., Paskievitch, J. F., Pourchet, M., Gow, A. J., Davis, M. E., and Kleinman, J.: Recent increase in South Pole snow accumulation, Annals of Glaciology, 21, 131–138, https://doi.org/10.3189/S0260305500015718, https://www.cambridge.org/core/product/identifier/S0260305500015718/type/journal_article, 1995.

Mosley-Thompson, E., Paskievitch, J. F., Gow, A. J., and Thompson, L. G.: Late 20th Century increase in South Pole snow accumulation, Journal of Geophysical Research: Atmospheres (1984–2012), 104, 3877–3886, https://doi.org/10.1029/1998JD200092, https://agupubs.onlinelibrary.wiley.com/doi/full/10.1029/1998JD200092, 1999.

Noël, B., Berg, W. J. v. d., Wessem, J. M. v., Meijgaard, E. v., As, D. v., Lenaerts, J. T., Lhermitte, S., Kuipers Munneke, P., Smeets, C. J. P. P., Ulft, L. H. v., Wal, R. S. W. v. d., and Broeke, M. R. v. d.: Modelling the climate and surface mass balance of polar ice sheets using RACMO2 – Part 1: Greenland (1958–2016), The Cryosphere, 12, 811–831, https://doi.org/10.5194/tc-12-811-2018, https://www.the-cryosphere.net/12/811/2018/, 2018.

Pettré, P., Pinglot, J. F., Pourchet, M., and Reynaud, L.: Accumulation distribution in terre adélie, antarctica: effect of meteorological parameters, Journal of Glaciology, 32, 486–500, https://doi.org/10.3189/S002214300001220X, https://www.cambridge.org/core/product/identifier/S002214300001220X/type/journal_article, 1986.

Picard, G., Brucker, L., Fily, M., Gallée, H., and Krinner, G.: Modeling time series of microwave brightness temperature in Antarctica, Journal of Glaciology, 55, 537–551, https://doi.org/10.3189/002214309788816678, http://openurl.ingenta.com/content/xref?genre=article&issn=0022-1430&volume=55&issue=191&spage=537, 2009.

Picciotto, E., Cameron, R., Crozaz, G., Deutsch, S., and Wiloain, S.: Determination of the Rate of Snow Accumulation at the Pole of Relative Inaccessibility, Eastern Antarctica: A Comparison of Glaciological and Isotopic Methods, Journal of Glaciology, 7,

273–287, https://doi.org/10.3189/S002214300003104X, https://www.cambridge.org/core/product/identifier/S002214300003104X/type/journal_article, 1968.

Rignot, E., Bamber, J. L., van den Broeke, M. R., Davis, C., Li, Y., van de Berg, W. J., and van Meijgaard, E.: Rignot, E. et al. Recent Antarctic ice mass loss from radar interferometry and regional climate modelling. Nature Geosci. 1, 106-110, Nature Geoscience, 1, 106–110, https://doi.org/10.1038/ngeo102, http://www.researchgate.net/publication/232802727_Rignot_E._et_al._Recent_Antarctic_ice_mass_loss_from_radar_interferometry_and_regional_climate_modelling._Nature_Geosci._1_106-110, 2008.

Rignot, E., Velicogna, I., van den Broeke, M. R., Monaghan, A. J., and Lenaerts, J. T.: Acceleration of the contribution of the Greenland and Antarctic ice sheets to sea level rise, Geophysical Research Letters, 38, L05 503, https://doi.org/10.1029/2011GL046583, http://doi.wiley.com/10.1029/2011GL046583, 2011.

Scambos, T. A., Frezzotti, M., Haran, T., Bohlander, J., Lenaerts, J. T., van den Broeke, M. R., Jezek, K., Long, D., Urbini, S., and Farness, K.: Extent of low-accumulation'wind glaze'areas on the East Antarctic plateau: implications for continental ice mass balance, Journal of Glaciology, 58, 633–647, http://www.ingentaconnect.com/content/igsoc/jog/2012/00000058/00000210/art00001, 2012.

Shepherd, A., Ivins, E. R., Geruo, A., Barletta, V. R., Bentley, M. J., Bettadpur, S., Briggs, K. H., Bromwich, D. H., Forsberg, R., Galin, N., Horwath, M., Jacobs, S., Joughin, I., King, M. A., Lenaerts, J. T., Li, J., Ligtenberg, S. R. M., Luckman, A., Luthcke, S. B., McMillan, M., Meister, R., Milne, G., Mouginot, J., Muir, A., Nicolas, J. P., Paden, J., Payne, A. J., Pritchard, H. D., Rignot, E., Rott, H., Sorensen, L. S., Scambos, T. A., Scheuchl, B., Schrama, E. J. O., Smith, B., Sundal, A. V., van Angelen, J. H., van de Berg, W. J., van den Broeke, M. R., Vaughan, D. G., Velicogna, I., Wahr, J., Whitehouse, P. L., Wingham, D. J., Yi, D., Young, D. A., and Zwally, H. J.: A Reconciled Estimate of Ice-Sheet Mass Balance, Science, 338, 1183–1189, https://doi.org/10.1126/science.1228102, http://www.sciencemag.org/cgi/doi/10.1126/science.1228102, 2012.

van de Berg, W. J. and Medley, B.: Brief Communication: Upper air relaxation in RACMO2 significantly improves modelled interannual SMB variability in Antarctica, The Cryosphere, 10, 459–463, https://doi.org/10.5194/tc-10-459-2016, http://www.the-cryosphere.net/10/459/2016/, 2016.

van de Berg, W. J., van den Broeke, M. R., Reijmer, C., and van Meijgaard, E.: Reassessment of the Antarctic surface mass balance using calibrated output of a regional atmospheric climate model, Journal of Geophysical Research: Atmospheres (1984–2012), 111, 159, https://doi.org/10.1029/2005JD006495, http://onlinelibrary.wiley.com/doi/10.1029/2005JD006495/full, 2006.

van Wessem, J. M., Reijmer, C., Morlighem, M., Mouginot, J., Rignot, E., Medley, B., Joughin, I., Wouters, B., Depoorter, M. A., Bamber, J. L., Lenaerts, J. T., De Van Berg, W. J., van den Broeke, M. R., and van Meijgaard, E.: Improved representation of East Antarctic surface mass balance in a regional atmospheric climate model, Journal of Glaciology, 60, 761–770, https://doi.org/10.3189/2014JoG14J051, http://openurl.ingenta.com/content/xref?genre=article&issn=0022-1430&volume=60&issue=222&spage=761, 2014.

van Wessem, J. M., van de Berg, W. J., Noël, B. P. Y., van Meijgaard, E., Birnbaum, G., Jakobs, C. L., Krüger, K., Lenaerts, J. T., Lhermitte, S., Ligtenberg, S. R. M., Medley, B., Reijmer, C. H., van Tricht, K., Trusel, L. D., van Ulft, L. H., Wouters, B., Wuite, J., and van den Broeke, M. R.: Modelling the climate and surface mass balance of polar ice sheets using RACMO2, part 2: Antarctica (1979-2016), The Cryosphere Discussions, pp. 1–35, https://doi.org/10.5194/tc-2017-202, https://www.the-cryosphere-discuss.net/tc-2017-202/, 2017.

Vaughan, D. G., Bamber, J. L., Giovinetto, M., Russell, J., and Cooper, A. P. R.: Reassessment of Net Surface Mass Balance in Antarctica, Journal of Climate, 12, 933–946, https://doi.org/10.1175/1520-0442(1999)012<0933:RONSMB>2.0.CO;2, http://journals.ametsoc.org/doi/abs/10.1175/1520-0442%281999%29012%3C0933%3ARONSMB%3E2.0.CO%3B2, 1999.

Venteris, E. R. and Whillans, I. M.: Variability of accumulation rate in the catchments of Ice Streams B, C, D and E, Antarctica, Annals of Glaciology, 27, 227–230, https://doi.org/10.3189/1998AoG27-1-227-230, https://www.cambridge.org/core/product/identifier/ S0260305500017493/type/journal_article, 1998.

Verfaillie, D., Fily, M., Le Meur, E., and Magand, O.: Snow accumulation variability derived from radar and firn core data along a 600 km transect in Adelie Land, East Antarctic plateau, The Cryosphere, 6, 1345–1358, https://doi.org/10.5194/tc-6-1345-2012, http://www. the-cryosphere.net/6/1345/2012/, 2012.

Vignon, E., Genthon, C., Barral, H., Amory, C., Picard, G., Gallée, H., Casasanta, G., and Argentini, S.: Momentum- and Heat-Flux Parametrization at Dome C, Antarctica: A Sensitivity Study, Boundary-Layer Meteorology, 162, 341–367, https://doi.org/10.1007/s10546-016-0192-3, https://link.springer.com/article/10.1007/s10546-016-0192-3, 2016.

Wang, Y., Hou, S., Sun, W., Lenaerts, J. T., van den Broeke, M. R., and van Wessem, J. M.: Recent surface mass balance from Syowa Station to Dome F, East Antarctica: comparison of field observations, atmospheric reanalyses, and a regional atmospheric climate model, Climate Dynamics, pp. 1–15, https://doi.org/10.1007/s00382-015-2512-6, http://link.springer.com/article/10.1007/s00382-015-2512-6/ fulltext.html, 2015.

Wang, Y., Ding, M., van Wessem, J. M., Schlosser, E., Altnau, S., van den Broeke, M. R., Lenaerts, J. T., Thomas, E. R., Isaksson, E., Wang, J., and Sun, W.: A Comparison of Antarctic Ice Sheet Surface Mass Balance from Atmospheric Climate Models and In Situ Observations, Journal of Climate, 29, 5317–5337, https://doi.org/10.1175/JCLI-D-15-0642.1, http://journals.ametsoc.org/doi/abs/10.1175/ JCLI-D-15-0642.1, 2016.